



Review

Bactericide effects of transparent polyethylene photocatalytic films coated by oxides under visible light

Sami Rtimi ^{a,b,*}, John Kiwi ^b^a Ecole Polytechnique Fédérale de Lausanne, Group of Advanced Oxidation Processes, EPFL-SB-ISIC-GPAO, Station 6, CH-1015, Lausanne, Switzerland^b Ecole Polytechnique Fédérale de Lausanne, Powder Technology Laboratory, EPFL-STI-IMX-LTP, Station 12, CH-1015, Lausanne, Switzerland

ARTICLE INFO

Article history:

Received 28 February 2017

Received in revised form 23 April 2017

Accepted 2 May 2017

Available online 4 May 2017

Keywords:

Photocatalysis

Thin films

Bacterial inactivation kinetics

Surface characterization

Sputtering

Innovative oxides

ABSTRACT

This review addresses catalytic/photocatalytic films under visible light inducing fast bacterial inactivation. These films present uniform, stable and adhesive surfaces able to inactivate bacteria within minutes. Uniform sputtered polyethylene-TiO₂ (PE-TiO₂) films absorbing mainly in the UV-region were later followed by studies on PE-FeOx and PE-FeOx-TiO₂ absorbing light in the visible region. The amount of TiO₂ sputtered on PE was significantly increased by RF-plasma pre-treatment due to the additional polar binding sites introduced on the PE-film. The hydrophobic to hydrophilic conversion of the PE-TiO₂ films under light irradiation was observed to be concomitant with the bacterial inactivation time. The TiO₂ diffuse reflectance spectra (DRS) of TiO₂-PE-films were extensively modified by the sputtering of FeOx. The structure of the sputtered layers revealed a random deposition of FeOx-TiO₂ on PE. The oxidative radical species generated on semiconductor surfaces were identified by appropriate scavenging experiments. By photoelectron spectroscopy (XPS), the redox processes occurring on the photocatalysts were evaluated. Repetitive bactericide cycling was possible for the three films discussed in this review. Bacterial inactivation mechanisms were suggested for the different films presented in this review.

© 2017 Elsevier B.V. All rights reserved.

Contents

1. Introduction	62
2. Transparent PE-TiO ₂ films absorbing incident light mainly in the UV-spectral region	63
3. Transparent PE-FeOx films absorbing in the visible region. synthesis and mechanistic features	67
4. Transparent PE-FeOx-TiO ₂ random layers inducing bacterial inactivation under visible light. Kinetics and mechanism	70
5. Conclusions	72
Acknowledgements	72
References	72

1. Introduction

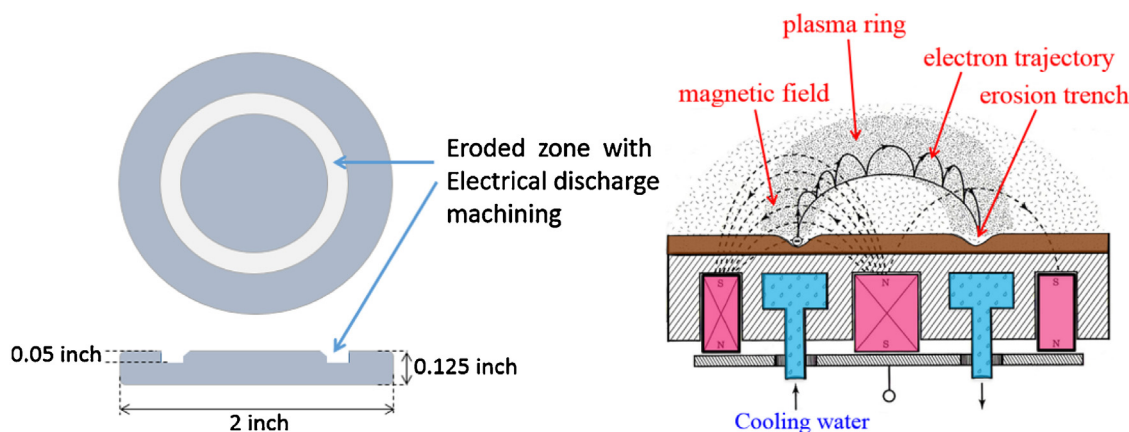
TiO₂ film preparation on glass, metal plates, textile fabrics and polymer films is a subject of timely research in the area of antibacterial films [1,2]. Sol-gel commercial methods are known for some decades to prepare TiO₂ thin films on heat resistant substrates [3–5]. But the thickness of the TiO₂ films was not reproducible, the films were not mechanically stable, and exhibited low

adhesion. The films can be wiped off by friction by applying a cloth or thumb [6]. Colloid deposition on substrates requires temperature of few hundred degrees for an adequate adherence to the selected substrate.

Radio Frequency plasma (RF-plasma) or UVC light were reported to induce an increase in the surface polar sites on polymers able to bind TiO₂ nanoparticles [7–9]. RF-plasma pretreatment increases the polarity, roughness and hydrophilicity (C–OH) of polymeric films improving its bondability and interfacial adhesion [10]. The largest increase in surface polarity has been reported for the surfaces presenting the highest O/C atomic ratio [11,12]. The RF-plasma pretreatment induces negatively charged functional groups, e. g., carboxylic, percarboxylic, epoxide and peroxide

* Corresponding author at: Ecole Polytechnique Fédérale de Lausanne, Group of Advanced Oxidation Processes, EPFL-SB-ISIC-GPAO, Station 6, CH-1015, Lausanne, Switzerland.

E-mail address: sami.rtimi@epfl.ch (S. Rtimi).



Scheme 1. Iron target artificially modified allowing DCMS FeOx deposition.

groups by the atomic O, excited O, anionic and cationic O generated in the RF-plasma chamber. The functionalized negative sites bind the slightly positive sputtered $Ti^{4+}/(TiO_2)$ through electrostatic attraction involving chelation/complexation.

Kelly et al., reported sputtering of TiO_2 films [14]. Parkin [15], Foster [23], Mills [16], Foster [17], Dunlop [18] and Yates [19] have deposited antibacterial TiO_2 films on glass by chemical vapor deposition (CVD). The disadvantage of CVD deposition is the high temperature required for the deposition requiring costly cooling systems. Polyethylene (PE) is a low cost and widely available material. It is chemically inert, mechanically stable and flexible, UV-resistant and does not oxidize in air under sunlight. For this reason, PE has been selected as the support for the TiO_2 , FeOx and FeOx- TiO_2 films reported in this review. The PE- TiO_2 films are designed to increase the quantum yield for light induced processes due to the transparency high refractive index [20].

Iron oxide nanoparticles (NP's) are of considerable interest due to their wide applications in fields such as magnetic storage, medicine, chemical industries, catalytic/photocatalytic materials and water purification [21,22]. FeOx films are at present an active area of research in biomaterials, protective coatings and medical bactericide devices [23,24]. The present review relates to the sputtering of FeOx films by direct current magnetron sputtering (DCMS) at temperatures compatible with the flowing point of the polymer substrate [25]. Depositing Fe via DCMS is not evident since the magnetic field generated from the magnets behind the target cannot go out from the Fe-target due to its para-magnetization. The target was modified by creating an artificial eroded zone in order to let the magnetic field pass through the target forcing the electrons to follow a hopping trajectory along the target (Scheme 1).

RF-plasma pretreatment of PE was seen to be necessary to fix additional amount of FeOx on the pre-treated PE. The first study specifically reporting RF-plasma pretreatment enhancing and modifying textile surfaces on artificial fibres was reported in detail by Bozzi et al. [12]. Scheme 2 shows the production of active oxygen species resulting from RF plasma under vacuum and up to atmospheric pressure.

It has been reported that TiO_2 subsequently attaches to the RF-plasma pretreated surface by exchange, impregnation, or electrostatic binding of positively loaded metal/metal oxide with the negatively charged $-COO^-$ and $-O-O^-$ functional groups introduced onto the pretreated surface [12,13,20].

During the last decades, iron oxide colloids have been reported as a photocatalyst able to inactivate *Escherichia coli* (*E. coli*) via photo-Fenton processes in aqueous suspensions [26–28]. Malato et al., attributed the wide use of iron oxides to the broad absorption bands driven by visible light; especially for iron-ligands complexes

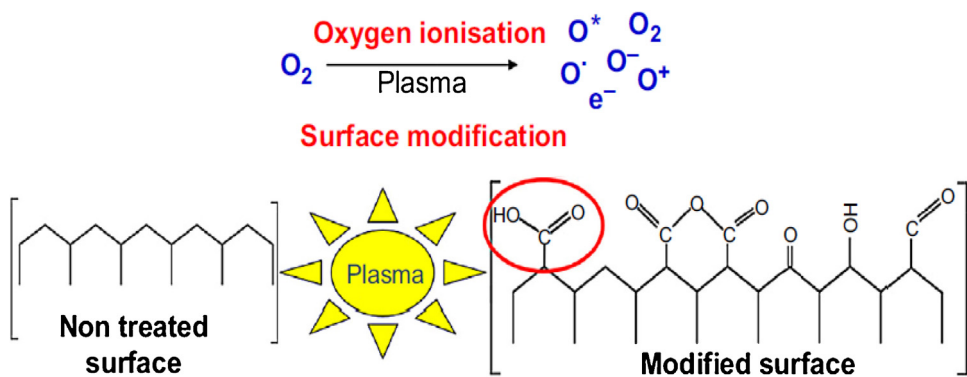
in aqueous media [26]. Ndounla et al., studied iron photo-assisted inactivation of wild enteric bacteria (total coliforms/*E. coli* and *Salmonella* spp.) in natural water (Sahelian wells) [27]. Furthermore, Ruales et al., studied the use of different iron oxides for water treatment [28]. The disadvantage of the catalysts/photocatalysts in suspension is the high cost needed for catalyst recovery. Deposition of metal-oxides nano-particulate films on different surfaces has been reported during the last decade [4,9,12].

Further development of Fe oxides (supported catalysts) is directed to find more effective, stable and kinetically faster Fe-based composites able to inactivate bacteria in shorter times. This kind of studies are warranted since the resistance of some bacteria to antibiotics is nowadays a serious health problem. It leads to increasing hospital-acquired infections (HAI) [29,30]. HAI present high care costs [31] and there is a need at the present time to produce antibacterial polymer films, rugs, curtains and medical devices. About 1.7 million HAIs occurred leading to almost 99,000 deaths in 2002. This makes HAIs the sixth leading cause of death in the USA and Europe. Recently Peleg and Hooper [32] reported that gram-negative (gram-) bacteria are responsible for more than 30% of HAIs, and these bacteria predominate in cases of ventilator-associated pneumonia (47%) and urinary tract infections (45%) and account for about 70% in intensive healthcare units.

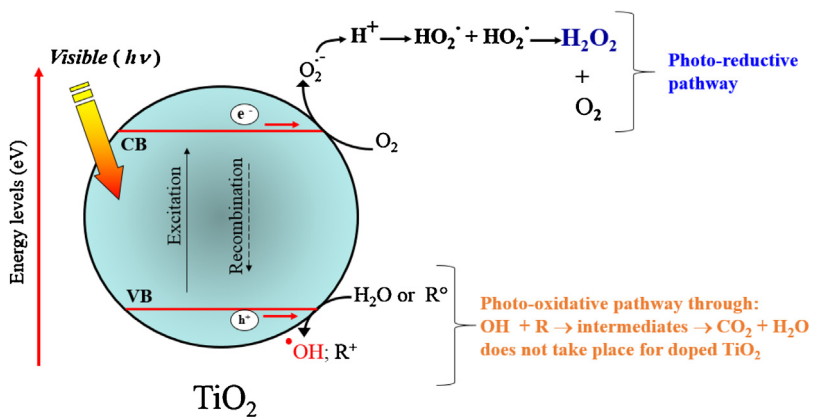
To increase the visible light absorption of TiO_2 the approach carried out was to couple a wide band-gap semiconductor with a narrow band-gap iron-oxide(s) semiconductor [33]. Bi-functional FeOx- TiO_2 compounds have recently shown an increased visible light absorption compared to bare TiO_2 leading to an accelerated degradation of arsenide [34], phenol [35] and 4-chlorophenol [36]. But no FeOx- TiO_2 bi-functional photocatalyst has been reported until now to inactivate bacteria under visible light irradiation. To deposit adhesive and uniform tunable FeOx- TiO_2 , FeOx and TiO_2 have been co-sputtered at relatively low temperature for relative short times on PE. This led to a random distribution of the FeOx and TiO_2 nanoparticles on the PE-surface [37]. The charge injection from the FeOx absorber into the TiO_2 under visible light was addressed and a mechanism of reaction was suggested [37]. Pumping the FeOx- TiO_2 in the visible range generates electron-hole pairs with a relaxation dynamic that was followed by transient absorption (TA) [38,39]. Until now, the FeOx- TiO_2 has been investigated by femto-second pump only in the UV-region [40].

2. Transparent PE- TiO_2 films absorbing incident light mainly in the UV-spectral region

During the last 4 decades TiO_2 has been used as the golden standard for semiconductor induced infection processes first in solution



Scheme 2. Plasma surface pretreatment.

Scheme 3. Radical production by the TiO_2 semiconductor surface under band-gap irradiation.

[1–3,21,22] and later deposited on suitable surfaces, and devices useful in the environmental and health sectors [5–9,23–25]. Under band-gap irradiation, the TiO_2 separates the conduction band electrons (from now $\text{cb}(\text{e}-)$) and valence band holes (from now $\text{vb}(\text{h}+)$) reacting with O_2 to produce highly oxidative radicals as show in Eq. (1) and Scheme 3.



The TiO_2 semiconductor was selected due to its stability, resistance to chemical corrosion, stability up to pH 13 and wide availability in purified form like the TiO_2 Degussa P-25.

Transparent surfaces (like polyethylene, PE) are important as wrapping materials. Over 60 million tons of poly(ethene), often known as polyethylene and polythene, are manufactured each year making it the world's most important plastic. Its uses include film, packaging (food packaging or as a packaging material of perishable commercial products marketed in the health sector) and containers, from bottles to buckets. PE has been reported to be a fruitful ground for bacterial incubation and reproduction [1–4,23–25]. This is the reason to develop kinetically fast, stable, robust, adhesive PE-films able to inactivate bacteria/fungi/pathogens under light and/or in the dark as it is discussed in this review. TiO_2 coatings have been deposited on cotton [9,12], polyester [7,8], polyamide [4], nylon [41] and other substrates using colloidal, sol-gel, dip-coating among of other routes. Supported TiO_2 was used for self-cleaning of coffee, wine, grease and dyes stains. Antibacterial activity of sol-gel and colloidal supported TiO_2 films was also investigated [42,43]. Although these preparations showed self-cleaning and self-sterilizing activities under UV light, the colloidal prepared TiO_2 coatings showed low adherence and reproducibility [13,20]. The

thickness of these coatings was not controllable and could be easily wiped-off [3,6,20].

Novel study on PE- TiO_2 sputtered transparent films addressed: a) the design, preparation, evaluation and characterization of innovative pretreated PE- TiO_2 films inactivating *E. coli*, b) the bacterial inactivation kinetics under solar simulated light concomitant with the time of the PE- TiO_2 hydrophobic-hydrophilic conversion, c) the electron microscopy and surface particle distribution of the TiO_2 nanoparticles on PE, d) the mechanism leading to bacterial death [20,13].

Fig. 1 shows the *E. coli* inactivation on PE- TiO_2 films under simulated solar light with an integrated light dose of 52 mW/cm^2 . The fastest bacterial inactivation was found for pretreated PE fabrics followed by TiO_2 sputtering for 8 min. Fig. 1a) presents the bacterial inactivation on PE- TiO_2 samples sputtered for 8 min and RF-pretreated for different times. No significant bacterial inactivation was observed for bacteria on uncoated PE (Fig. 1a, trace 4). Only trace 1) was subjected to statistical analyses since it showed the most favorable kinetics and presents the highest amount of TiO_2 sites in exposed positions interacting with bacteria. PE- TiO_2 sputtered for 1 and up to 5 min did not contain sufficient TiO_2 to drive a fast bacterial inactivation.

The determination of bacteria was carried out basically by reactions at the solid-air interface as shown by the experimental setup shown below in Fig. 1b. A 100 microliter saline solution containing the *E. coli* were spread on the PE. The light source inside the solar simulated light cavity was located perpendicular to the samples. The PE used shows an absorption $<250 \text{ nm}$ and TiO_2 absorbs below 385 nm . This information has been widely reported in the literature [1–5]. The PE- TiO_2 film transmission depend on the amount of sputtered TiO_2 .

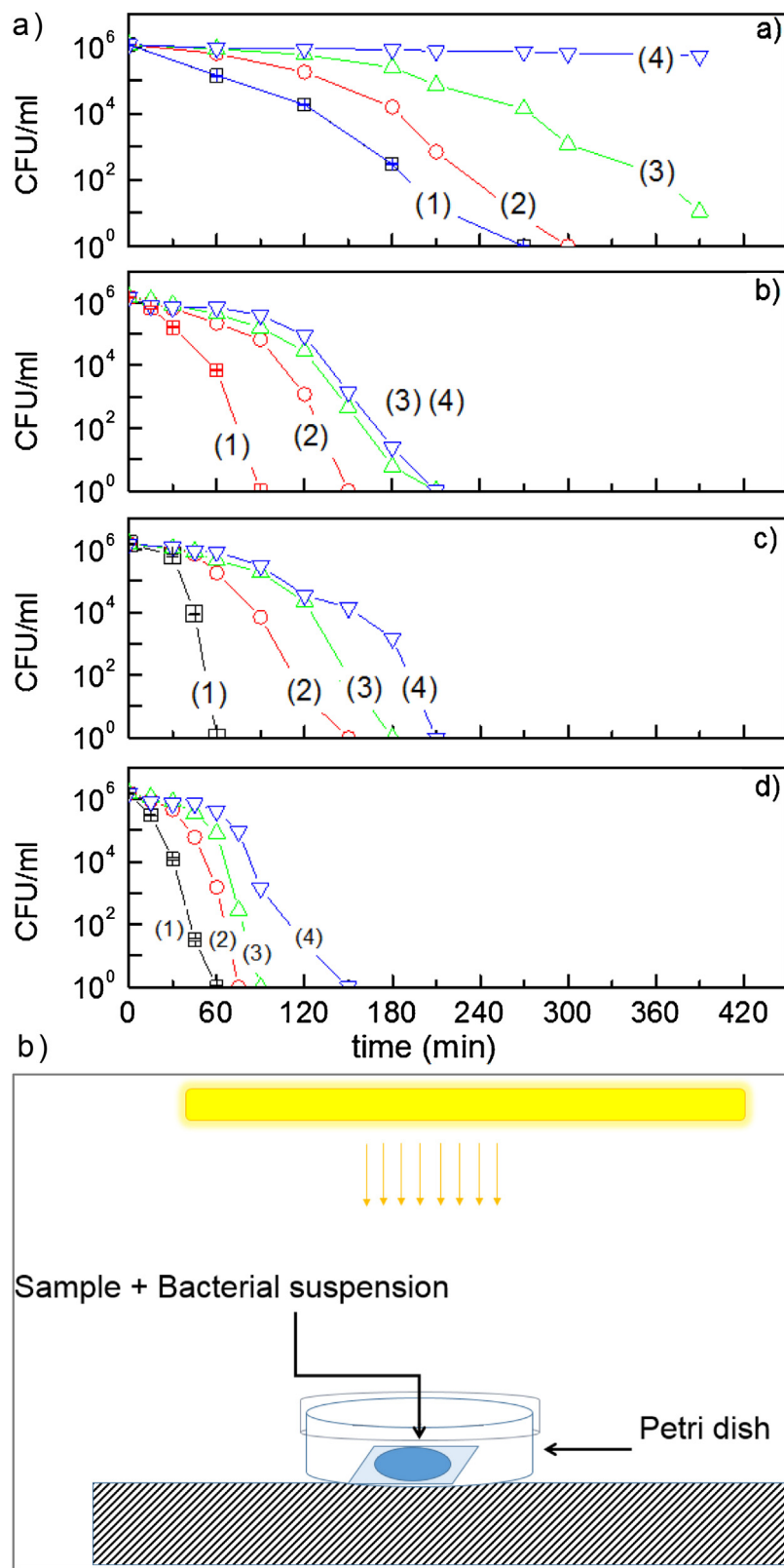


Fig. 1. (a) *E. coli* inactivation on *TiO*₂ sputtered on PE for 8 min irradiated with simulated solar light (52 mW/cm²) a) *TiO*₂ sputtered for different times without RF-plasma pretreatment for: (1) 8 min, (2) 10 min, (3) 5 min and (4) PE alone. b) *TiO*₂ sputtered for 8 min with surface RF-plasma pretreatment at 1 Torr for times: (1) 15 min, (2) 20 min, (3) 30 min and (4) 5 min c) *TiO*₂ sputtered 8 min RF air plasma pre-treatment for: (1) 15 min, (2) 20 min, (3) 30 min and (4) 5 min d) *TiO*₂ sputtered 8 min with UVC pretreatment for: (1) 20 min, (2) 15 min, (3) 10 min and (4) 5 min [20]. Error bars: SD, $\sigma = 5\%$. (b) Experimental set-up to evaluate the bacterial inactivation kinetics under light irradiation.

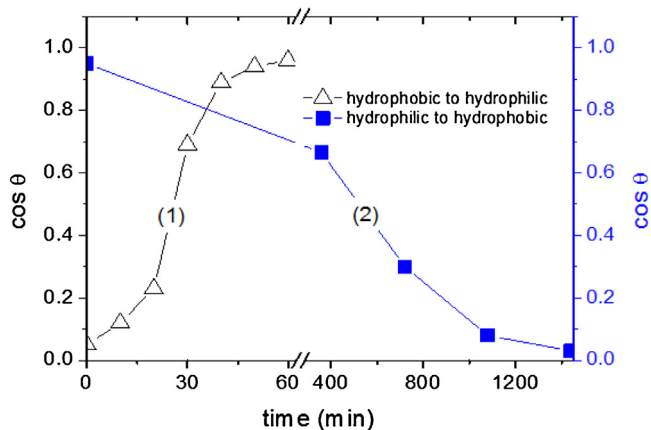


Fig. 2. (1) Kinetics of the hydrophobic-hydrophilic transformation under solar simulated light of a film pretreated by RF-air plasma for 15 min and sputtering for 8 min at times up to one hour and (2) kinetics of the dark reverse reaction to the initial state for PE-TiO₂ film RF-air plasma pretreated for 15 min and sputtered for 8 min.

The Ti-loading on PE was determined by X-ray fluorescence (XRF) at times 1, 3, 5 min and the values found were 0.009, 0.019 and 0.031 TiO₂ wt%/wt PE respectively. Samples sputtered for times longer than 8 min led to layer thickness >60 nm. Higher thicknesses lead to the bulk inward diffusion of charges decreasing the charge transfer between the PE-TiO₂ and bacteria [20,28,44,45]. Sputtering for 8 min led to a TiO₂ loading with the most suitable thickness for the charge diffusion able to reach bacteria in Fig. 1c, trace (1). No bacterial inactivation was observed for bacteria on PE films in the dark. To verify that no re-growth of *E. coli* occurs after the first bacterial inactivation cycle, the PE-TiO₂ film was incubated on an agar Petri dish for 24 h at 37 °C. No bacterial re-growth was observed meaning that there were no bacteria present on the surface after the inactivation cycle.

A further proof for the bacterial inactivation is related to the unambiguous identification of the lipid peroxidation of the outer cell bacterial membranes like lipo-polysaccharides (LPS). Peroxidation is due to unsaturated lipid chains in the LPS reacting with molecular oxygen to yield lipid hydro-peroxide and dialkyl-peroxides leading to the formation of malondialdehyde (MDA) [28,45]. The increase in MDA generation was observed to be concomitant to the increase in hydrophilicity photo-generated on PE-TiO₂ under solar simulated light irradiation [20,13].

Supported films coated with TiO₂ either by colloidal means or by sputtering [1–11] have been shown photo-switching under band-gap irradiation from a hydrophobic state to a highly hydrophilic state under band gap irradiation by a notable amount of well-known papers [45–47]. This property is concomitant and occurs during the production of highly reactive radicals produced at the surface of TiO₂ leading to bacterial abatement. Sometimes the hydrophobic-hydrophilic transformation occurs during the time of bacterial inactivation [20]. Sometimes this is not the case, generally the hydrophobic to hydrophilic transformation is faster than the bacterial inactivation time. The hydrophobic to hydrophilic transformation occurring on the sputtered PE-TiO₂ samples induced by simulated solar light have been investigated by many research groups [13,20,45–47]. Rtimi et al., recently reported a decrease of the contact angle to less than 5° within 60 min during the bacterial inactivation time. Authors followed also the recovery from the PE-TiO₂ photo-induced hydrophilic surface to the initial hydrophobic surface proceeding within 24 h in the dark [13].

Fig. 2 illustrates the rate of photo-induced hydrophilicity and the back reaction to the initial hydrophobic PE-TiO₂ surface as a function of “cos θ”. The induced hydrophilicity by the light irradiation on the PE-TiO₂ samples is shown in Fig. 2, trace 1. The back-reaction

from hydrophilicity to the initial hydrophobicity on PE-TiO₂ in the dark, is shown in Fig. 2, trace 2.

According to Young's theory the “cos θ” of a liquid droplet on a solid surface is a function of the interfacial energy between the solid and the liquid. The contact angle conventionally measures the angle where the liquid meets the solid quantifying the wettability of a solid surface via the Young equation. The Young equation involves solid-vapor, liquid-vapor and solid-liquid interfacial energies. The solid-vapor interfacial energy is denoted by γ_{SG} , the solid-liquid interfacial energy by γ_{SL} , and the liquid-vapor interfacial energy i.e. the surface tension by γ_{LG} , then the equilibrium contact angle θ_C is determined from these quantities by Young's equation:

$$0 = \gamma_{SG} - \gamma_{SL} - \gamma_{LG} \cos \theta_C \quad (2)$$

In Eq. (2), the surface free energy and $t = \infty$ corresponds to interfacial energy of the hydrophobic surface before irradiation. The rate of the hydrophobic to hydrophilic conversion and the reverse reaction were: 0.277 min⁻¹ and 8.71×10^{-3} min⁻¹ respectively [20,13]. During the irradiation the hydrophobic surface is converted to a hydrophilic surface reducing the interfacial energy between the solid and liquid surface. Seki and Tachiya [47] optimized this equation taking into account the difference in interfacial energy and the equation becomes:

$$\cos \theta = (\gamma_{SG} - \gamma_{SL}) / \gamma = (\gamma_1 C + \gamma_1) / \gamma f_1 C + f_2 \quad (3)$$

where: $f_1 = \gamma_1 / \gamma$, $f_2 = \gamma_2 / \gamma$ and C is the surface fraction of hydrophilic region.

Fig. 3a–d shows the electron microscopy images for PE-TiO₂ RF-plasma pretreated for 15 min (in near-atmospheric pressure) and sputtered for 8 min, inducing the faster bacterial inactivation as seen in Fig. 1. Fig. 3a show a continuous coating of TiO₂ on PE. TiO₂ thickness of ~60 nm is equivalent to 300 layers, taking an atomic layer thickness of 0.2 nm [20]. Fig. 3b shows the High Angle Annular Dark Field (HAADF) mode. The uniform distribution obtained by Energy-dispersive X-ray spectroscopy (EDX) of O and Ti on the coating is shown in Fig. 3c and d. Fig. 3 shows the TiO₂ is dispersed uniformly over the PE-surface.

A model for bacterial inactivation of *E. coli* under light irradiation is suggested in Fig. 4, and variations of this model have been generally cited widely for the bacterial disinfection/mineralization mediated by TiO₂ photocatalysis [1,2,16,21,23]. The intrinsic light absorption by TiO₂ induces the transition 2p (O) → 3d (Ti).

The photo-generated electrons and holes interact with surface adsorbed molecules such as water and oxygen to form active radicals so called reactive oxygen species (ROS). The catalytic reaction of the TiO₂ involves the water, dissolved oxygen and the catalyst surface groups [1–7]. Indeed, they are summarized in Eqs. (4) and (5):



At the molecular level, the photo-generated electrons tend to reduce Ti⁴⁺ to Ti³⁺ and the holes react with the bridging oxygen sites leading to oxygen vacancies and free ${}^{\circ}OH$ -radicals. Water molecules heal the oxygen vacancies producing OH-groups on the surface leading to the oxidation of Ti³⁺ into Ti⁴⁺ [7].

The performance of a TiO₂ can be improved as to increase the light absorption in the visible region by doping. Recent reports showed that associating Ag and/or Cu oxides with other metal oxides hinders the photo-generated charges recombination through the introduction of intra-gap energy level midway between the conduction band (cb) and the valence band (vb) of TiO₂ facilitating the indirect transition of the electron through the forbidden band [36,48,49].

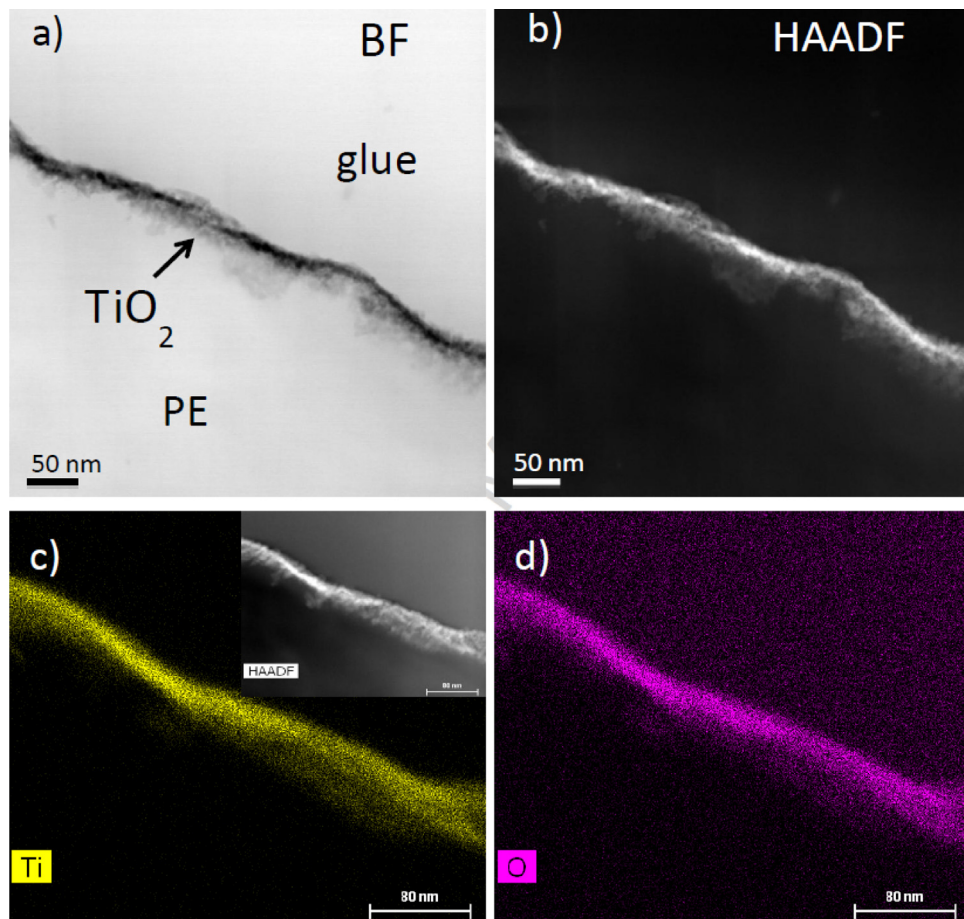


Fig. 3. a) STEM Bright Field Image of PE-TiO₂ RF air-plasma pretreated for 15 min and TiO₂ sputtered for 8 min, b) STEM-HAADF image taken on the same sample area, c) EDX mapping of titanium and d) EDX mapping of oxygen.

3. Transparent PE-FeOx films absorbing in the visible region. synthesis and mechanistic features

Iron oxides (FeOx) have been reported as useful semiconductor oxides mainly in solution leading to bacterial inactivation [1–3,21–24]. It has the advantage to absorb light in the visible region up to 560–570 nm depending on the variety of the iron oxide selected for the task.

Iron-oxides photo-assisted Fenton system is one of the most popular and widely studied advanced oxidation processes (AOPs). Photo-Fenton system ($\text{Fe}^{2+}/\text{Fe}^{3+}/\text{H}_2\text{O}_2/\text{hv}$) has been reported to significantly increase the inactivation rate of the enteric bacteria contents of the water wells. Pulgarin et al., recently reported that iron naturally present in the well water influences the reaction mechanism of $\text{H}_2\text{O}_2/\text{hv}$ by favoring the photo-Fenton process in natural wells in rural areas [27]. The oxidation of ferrous iron by hydrogen peroxide generates highly oxidative species especially hydroxyl radical ($\cdot\text{OH}$). Ferrous iron, in the absence of hydrogen peroxide, has the tendency to rapidly be oxidized and form different aqua- Fe^{3+} species, depending on the pH levels of the medium as recently reported [28].

Membrane related research has attracted much attention in recent years as a structured medium for a variety of chemical reactions [13,20,43]. Nafion perfluorinated membranes have been used during the last decade in a variety of catalytic/electro-catalytic integrated chemical reactions [50,13]. The degradation of non-biodegradable azo-dye Orange II by photo-Fenton reactions in Fe-free solutions. This dye does not undergo bacterial degradation in a waste-water treatment plant due to the aromatic and

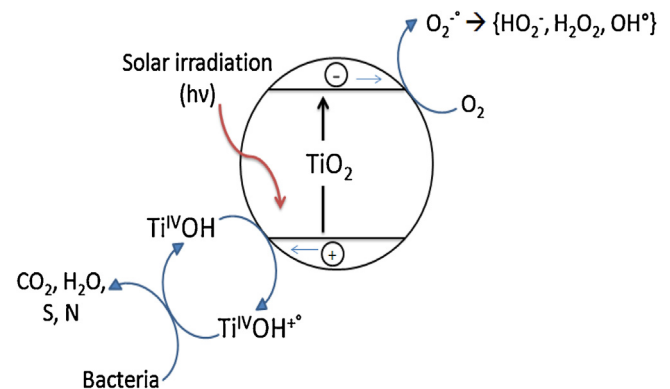
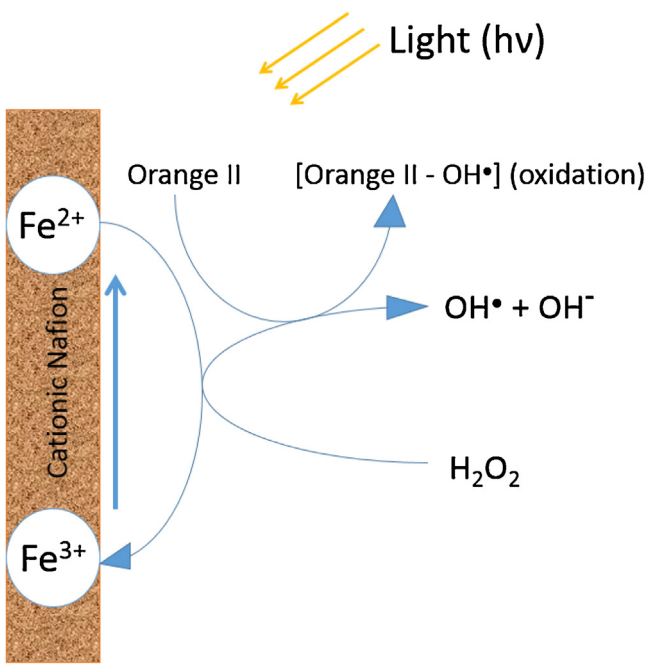


Fig. 4. Suggested model for the bacterial inactivation on PE-TiO₂ films under solar simulated light irradiation.

sulfo-aromatic group found in the ring structure. Azo dyes, which account for more than 20% of industrial dye production, are commonly found in effluents of the textile industry. The disappearance of Orange II (pH 2.8) under light irradiation on a Fe-loaded Nafion membrane by a Suntest lamp was recorded as a function of time for different concentrations of H_2O_2 in the solution as shown in Scheme 4. With increasing concentration of H_2O_2 the Orange II degradation kinetics was accelerated. At H_2O_2 concentrations >0.8 mm, no further degradation acceleration was observed. This effect is due to the known scavenging effect when using higher



Scheme 4. Degradation of Orange II in acidic solutions due to the photo-production of oxidative radicals in solution on Nafion/Fe³⁺/Fe²⁺-cationic membranes.

H₂O₂ concentration on the further generation of hydroxyl radicals in solution [51].

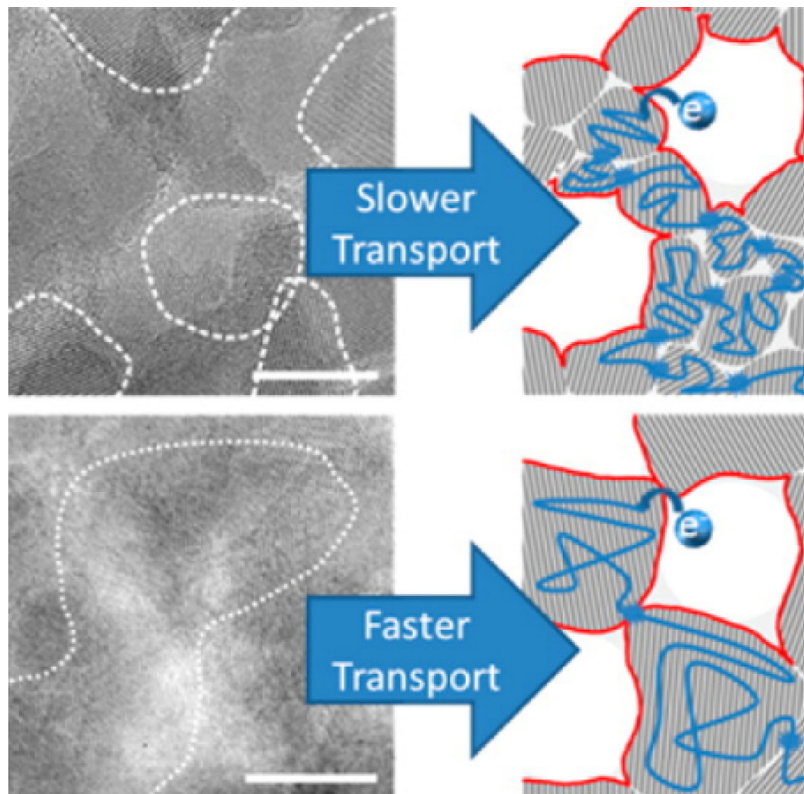
Antibacterial features of PE-FeOx films prepared on RF-plasma pretreated PE followed by sputtering of Fe in a reactive O₂ atmosphere was recently studied [25]. The latter work accounted in detail on the evaluation of the *E. coli* inactivation kinetics, the

mechanism of bacterial inactivation on PE-FeOx surfaces, bacterial adhesion and the characterization of the PE-FeOx film microstructure [25].

E. coli inactivation under solar simulated light and in the dark by RF-pretreated samples with different Fe-loadings have been reported [25]. PE-FeOx sputtered for 60 s were seen to lead to the faster bacterial inactivation. Bacterial inactivation was seen to not take place in the dark on PE-FeOx films nor does it proceed on PE alone under simulated solar irradiation. Sputtering times of 120 and 150 s led to longer bacterial inactivation times. This was attributed to two effects: a) the increase in layer thickness leading to bulk inward diffusion of the charge carriers [20,49] and b) the size of the FeOx-clusters increased with the sputtering time. This leads to FeOx agglomerates, but the catalytic activity per exposed atom would consequently decrease due to agglomeration. Snaith et al., [52] recently studied the charge transfer/transportation in a nano-particulate layer. The charge transfer/transport was limited by the size of the grains forming the thin layers without taking into account the variability of the inter-particles contact area as shown in **Scheme 5**.

During the last two decades, many studies reported the deposition on glass of TiO₂, TiO₂-Ag, and TiO₂-Cu by CVD [14–19]. During the deposition process it was observed that the size of the metal/oxide particles on the support were a function of the coating thickness and determined the roughness of the topmost layers as well as the particle adhesion on the antibacterial films [53]. Since the charge separation in time and space is a function of the particle size in oxides and composite materials, the mobility of the conduction band electrons will be certainly controlled by the particle size, shape, geometry and crystallographic phase as suggested in references [32,44,54].

Bacterial adhesion on different surfaces has become a significant problem in industry [53], public places and health facilities associated with toxic pathogenic bacteria [25]. Bacterial attachment to



Scheme 5. Mobility of conduction band electrons influenced by grain boundaries [52].

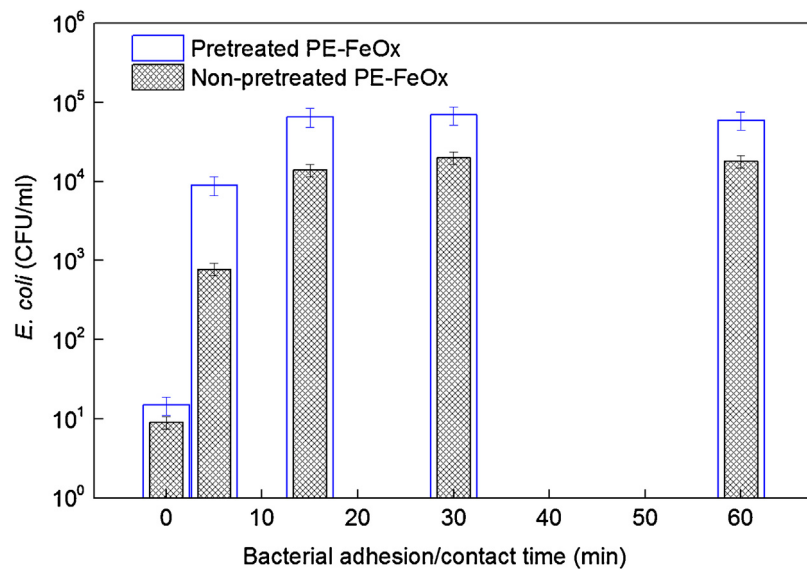


Fig. 5. *E. coli* adhesion on PE-FeOx sputtered for 60s: (□) RF-plasma pre-treated surface for 15 min and (■) PE-FeOx sputtered for 60 s non-pre-treated surface. Error bars: SD, $\sigma = 5\%$.

a surface is a complex process regulated by diverse characteristics of the growth medium, substratum and the bacterial cells by themselves. These surfaces act as a pump generating and spreading dangerous infections.

Bacterial adhesion has recently been followed as a function of the contact time with PE-FeOx (without pretreatment) compared to pre-treated PE-FeOx and the results are shown in Fig. 5 [25]. The diffusion of the highly oxidative radicals (ROS) by the PE-FeOx film under sunlight led to the abatement of the adhered or the weakly adhered bacteria. Radicals leading to the bacterial inactivation by PE-FeOx were investigated using appropriate scavengers. Scavenging the OH-radicals with Dimethylsulfoxide (DMSO) slows down bacterial inactivation but this effect seems not to be significant since the bacterial inactivation was slowed down in a very limited way. More important is the almost complete suppression of the bacterial inactivation by Ethylenediaminetetraacetic acid (EDTA-2Na) scavenging the valence band holes $vb(h^+)$. The addition of Superoxide dismutase (SOD) was used to detect the HO_2/O_2^- . Both scavengers (EDTA-2Na and SOD) preclude almost entirely the bacterial inactivation. This means that the major actors leading to bacterial inactivation on sputtered FeOx-PE are HO_2/O_2^- and $vb(h^+)$; a minor implication was attributed to $^{\circ}OH$ [25].

Net we turn the attention to the change in the redox states before and after bacterial inactivation as detected by X-ray photoelectron spectroscopy (XPS). Fig. 6 presents the changes in the Fe-oxidation states of PE-FeOx within the 120 min bacterial inactivation period. The initial Fe(III) peak of Fe_2O_3 at 712.2 eV decreases from ~80.0% at time zero to ~53.0% after the time of bacterial inactivation. Concomitantly, an increase in Fe_3O_4 at 713.6 eV and Fe(II) with peaks at 709.7 eV was observed. The Fe-peaks have been referenced by the values reported in reference [55] corrected for electrostatic charging effects [56,57]. The changes in the surface atomic concentration percentages of Fe, C and O [54,55] reflect redox processes shifting the Fe peaks. After bacterial inactivation, the XPS peak positions for the Fe(III), $FeO(II/III)$ and Fe(II) peaks were: 711.4 eV; 711.4 eV; 708.6 eV and 713.8 eV respectively. The three Fe-oxides in Fig. 6 offer different potential-pairs to catalyse the bacterial reduction [25]. No accumulation of residual intermediates on the catalyst after bacterial inactivation takes place since no accumulation was found of the C-content on the catalyst surface.

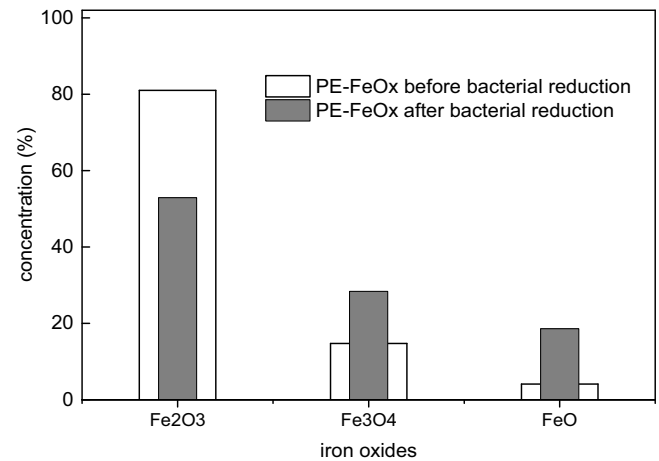


Fig. 6. XPS investigation of iron oxide oxidation states on the PE-FeOx surfaces sputtered for 60 s before and after bacterial inactivation under solar simulated light (52 mW/cm²).

A mechanism for the bacterial inactivation on sputtered PE-FeOx films was suggested in Fig. 7 [25]. The electrostatic attraction of the negatively charged *E. coli* at pH between 3 and 9 and the slightly positively charged PE-FeOx due to the Fe dense electronic charge at distances below 4 Å polarizes the interaction between both species within this short distance [58].

Fe_2O_3 presents a cb at +0.1 eV and a vb at +2.2 eV. The $vb(h^+)$ interact with the adsorbed $-OH$ surface groups but do not have the high potential to lead to the formation of OH° -radicals. The HO_2° -radicals oxidize bacteria undergoing HO_2°/HO_2^- reduction at 0.75 eV, a much lower potential compared to the potential required to drive the reaction OH°/OH^- of 1.90 eV [59]. The Fe_3O_4/FeO produced in this first step in Fig. 6 subsequently re-oxidizes to Fe_2O_3 in aerobic media. The conduction band of Fe_2O_3 at +0.1/0.2 eV is at a more positive potential than the potential required for the one electron oxygen reduction $O_2 + H^+ + e^- \rightarrow -0.22$ eV. This precludes the consumption of H^+ and the H^+ to drive the local pH towards more acidic values [25]. The HO_2° decomposes at pH > 4.8, driving the local pH to a more acidic local pH:



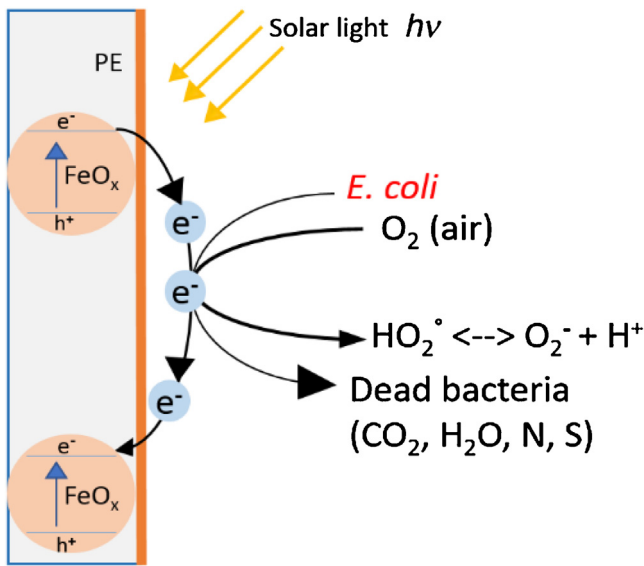


Fig. 7. Mechanism suggested for the bacterial inactivation mechanism under solar simulated light on PE-FeOx sputtered surfaces.

4. Transparent PE-FeOx-TiO₂ random layers inducing bacterial inactivation under visible light. Kinetics and mechanism

The development of a TiO₂ materials with a higher visible light response and concomitantly not decreasing the TiO₂ performance significantly to the TiO₂ performance under UV-light is the central problem in the field of TiO₂ related TiO₂ photocatalytic research. Many research groups have extensively doped TiO₂ with various transition metals and also more recently with anions [9,14–19,36]. Iron seems a suitable candidate to extend the TiO₂ absorption to into the visible because it is biocompatible, and abundant in nature. However, the positive doping effect is only limited to TiO₂ particles smaller than 10 nm in diameter as reported by Litter et al., and later by Nagaveni et al., [60,61]. Recently, Zhou et al., reported the use of ordered mesoporous TiO₂ in the fields of catalysis, energy storage and conversion, nano-reactors and gas sensors, due to their large surface area and ordered pore networks [62]. They reported

ordered mesoporous TiO₂ showing better photocatalytic activity than that of Degussa/Evonik P25 TiO₂ for degradation of highly toxic 2,4-dichlorophenol under UV irradiation. This enhancement was attributed to the well-ordered large-pore porous structure, which facilitates mass transport. The large surface area offering more active sites, and high crystallinity that favors the separation of photo-generated electron-hole pairs. Furthermore, mesoporous black TiO₂ materials with a highly ordered hexagonal mesostructure and a relatively high surface area were reported to exhibit high photocatalytic activity [63].

Using supported photocatalyst films, there is no-need for the catalyst recovery after the catalytic/photocatalytic process. For this reason, photoactive surfaces for self-cleaning and self-sterilizing purposes have recently been developed [9,12,25]. These works involved also the coupling of wide and narrow band-gap semiconductors leading to a higher light absorption in the visible region [64,65].

In this section, uniform, adhesive and reproducible PE-FeOx-TiO₂ film obtained by sputtering and leading to bacterial inactivation under visible light is described [37]. In this work, several features were addressed: a) the surface spectral properties of the PE-FeOx-TiO₂, b) the nature of the PE-FeOx-TiO₂ transients femto-second laser pulses induced in the visible light region (545 nm/25 fs), c) the bacterial inactivation kinetics of *E. coli* under low intensity solar simulated light/visible light and when different irradiation intensities were applied on the PE-FeOx-TiO₂ film and d) the mechanism of electron transfer from the photosensitized FeOx to the low lying TiO₂ trapping states [66].

The diffuse reflectance spectra (DRS) in Fig. 8 suggest that the hematite is the main component in the mixtures of iron-oxides (FeOx). This is due to similarity of both spectra as shown in Fig. 8, trace 2 & 3 [66,37]. This study shows that the spectrum of the PE-TiO₂ sputtered for 8 min is significantly lower compared to the PE-FeOx samples sputtered for 2 min.

The molar absorption coefficient Fe (III)/(Fox) species $\varepsilon = 1000 \text{ M}^{-1}\text{cm}^{-1}$ at 366–375 nm is considerably higher compared to TiO₂. The spectrum amplitude of Fe₂O₃ between 250 and 500 nm has been reported to be a function of the film thickness and grain size. In Fig. 8 the addition of the spectra reported by traces (1) of TiO₂-PE and (2) of FeOx-PE do not add up to trace FeOx-TiO₂-PE (3). This is the evidence for the formation of a new composite not corresponding to TiO₂ or FeOx [37,20,25]. The shift of the

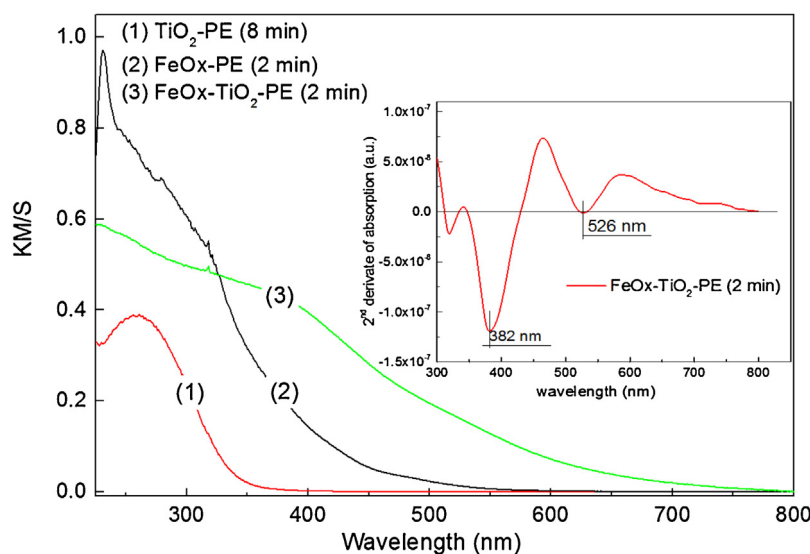


Fig. 8. Diffuse reflectance spectroscopy (DRS) of samples: (1) TiO₂-PE sputtered for 8 min, (2) FeOx-PE sputtered for 2 min and (3) FeOx-TiO₂-PE co-sputtered for 2 min. The insert shows the second derivative of the bands in the spectrum of FeOx-TiO₂ with their peak positions at 382 nm and 526 nm.

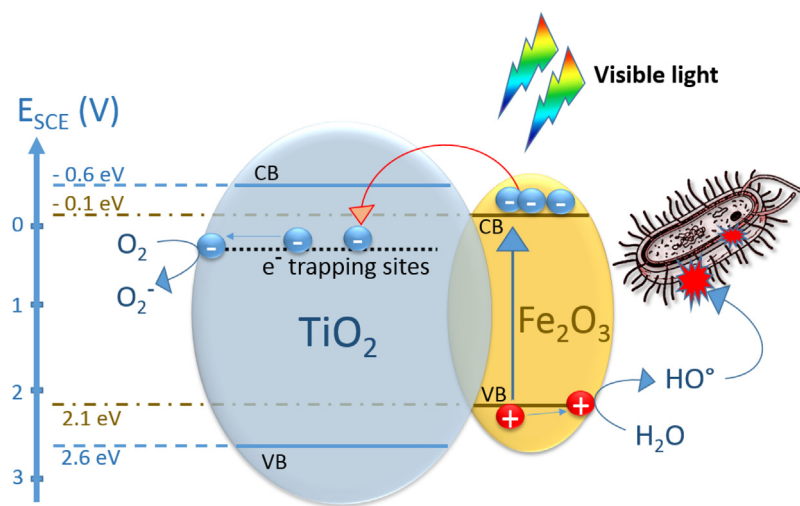
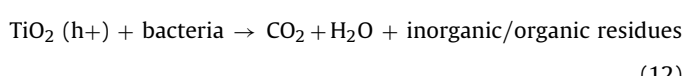
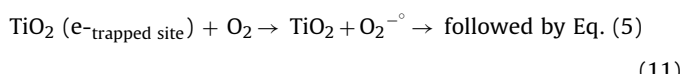
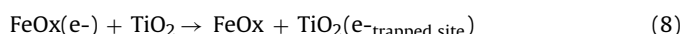
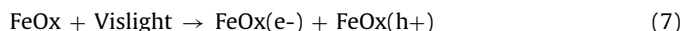


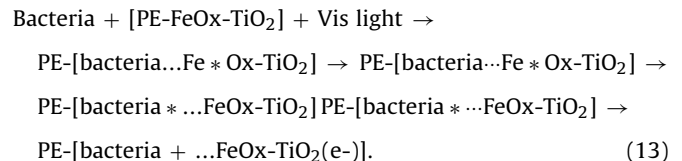
Fig. 9. Suggested electron transfer from the photosensitized FeOx to the low- lying TiO₂ trapped states.

spectrum in trace (3) to longer wavelengths upon addition of FeOx involves the incorporation of Fe(III) into the TiO₂ giving rise to additional Ti-Fe charge transfer bands. The formation of additional FeOx transfer bands cannot be discounted. Furthermore, when the FeOx-TiO₂ was cosputtered for 3 min, the optical absorption in Kubelka-Munk units was similar to the band obtained by films cosputtered for 2 min. This suggests that when co-sputtering for longer times, the FeOx chromophore did not drastically increase the absorbance, lending further support that a new FeOx-TiO₂ composite was sputtered on PE. The insert in Fig. 8 shows the second derivative of the FeOx-TiO₂ spectrum with two bands at 382 nm and 526 nm, the two light absorption maxima [37].

The bacterial inactivation kinetics was followed by plate counting [37]. *E. coli* bacterial inactivation kinetics by PE-FeOx-TiO₂ co-sputtered samples for 2 min led to the fastest bacterial inactivation (60 min) under simulated solar light (310–800 nm). The bacterial inactivation on PE-FeOx sputtered for 1 min was reported to take longer time (within 120 min) [25,37]. This is a faster bacterial inactivation time compared to films with thicker PE-FeOx coatings. The latter coating presented: a) an increase in the layer thickness leading to bulk inward diffusion of the charge carriers and b) FeOx-clusters with larger size (agglomerates) causing a decrease in the catalytic activity per exposed atom. The PE-FeOx-TiO₂ films shows a slower kinetics due to the low fraction of the sunlight absorbed by TiO₂ (< 390 nm) compared to FeOx. Bacterial inactivation does not proceed on PE under sunlight nor in the dark. The mechanism of reaction between PE-FeOx-TiO₂ and bacteria under visible light is suggested below by Eq. (7) through to Eq. (12).



An alternative shorthand notation for the visible light induced bacterial inactivation could be suggested below in Eq. (13):



The bacteria (RH) interacts with the $\text{TiO}_2\text{vb}(\text{h}^+)$ within the time of the laser pulse and competes with the charge recombination reaction $\text{e}^- + \text{h}^+ \rightarrow \text{decay}$. The fast bacterial inactivation kinetics on PE-FeOx compared to PE-FeOx-TiO₂ was attributed to two effects: a) the electron transfer from the photo-sensitizer FeOx to lower lying TiO₂ trapping states [65–71] and b) the formation of additional FeOx interfacial sites active in bacterial oxidation. Leytner et al., [67] showed by time-resolved photo-acoustic spectroscopy (TRPAS) the existence of electron trapping sites within anatase TiO₂ positioned 0.8 eV below the anatase cb. Hurum et al., [68] used electron paramagnetic resonance (EPR) spectroscopy to study the charge transfer to the mixed TiO₂ anatase-rutile interface. They reported that even though the rutile cb is ~0.2 eV lower than the anatase cb, the electrons can transfer from rutile cb to electron trapping sites of anatase located ~0.8 eV lower than the anatase cb. Visible light >400 nm cannot photo-induce electron-hole pairs on TiO₂ [37]. Pairs can only be induced by FeOx since the cb band of Fe₂O₃ is located at 0.5–0.8 eV lower compared to the cb of TiO₂ [70]. The e- acceptor role of the TiO₂ trapping-states in the PE-FeOx-TiO₂ cosputtered films leading to bacterial degradation under sunlight irradiation has been recently reported by Nadtochenko et al., [71].

The effect of the visible light (solar simulated light + filter/cut-off at 400 nm) irradiation on bacterial inactivation compared to the full solar simulated irradiation (310–800 nm) was also investigated by Rtimi et al., [37]. The *E. coli* inactivation kinetics under full solar spectral light or under visible light >400 nm was seen to be similar. Therefore, the more energetic photons between 310 and 400 nm do not lead to any significant acceleration of the bacterial inactivation. This unexpected result lent further support to the predominant role of FeOx as the photo-sensitizer during the bacterial inactivation by PE-FeOx-TiO₂ films. Bacterial inactivation kinetics as a function of the applied sunlight doses showed that a light dose of 50–70 mW/cm² led to bacterial inactivation within 60 min. Lower light dose (30 mW/cm²) led to slower bacterial inactivation. This

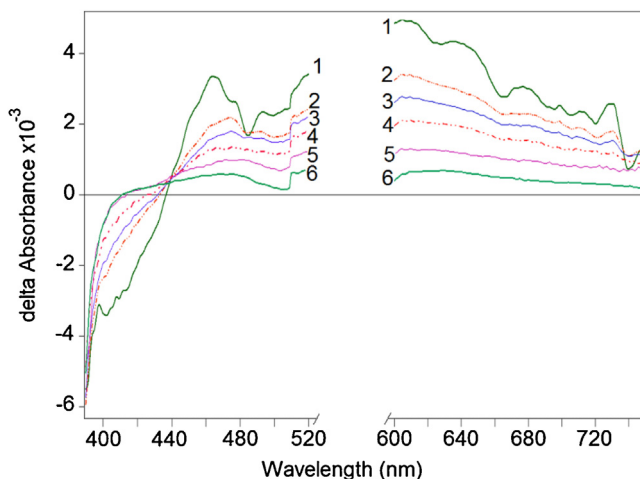


Fig. 10. Transient spectra of the FeOx-TiO₂-PE as a function of wavelength after femtosecond laser pulse 25 fs (544 nm). Time delays: 1) 150 fs; 2) 500 fs; 3) 1 ps; 4) 3 ps; 5) 10 ps; 6) 500 ps.

confirms the FeOx-TiO₂-PE acting as a semiconductor during bacterial inactivation. Electron transfer from the photo-sensitizer FeOx to lower lying TiO₂ trapping states was suggested as the bacterial inactivation mechanism. This mechanism is shown schematically in Fig. 9.

Femto-second ultra-fast kinetics is a powerful tool to detect the initial charge separation within very short times when PE-FeOx-TiO₂ is irradiated under visible light. We have used femto-second kinetics pulses in the visible range (545 nm/25 fs) to photo-induce and identify the transients obtained by absorption spectroscopy of FeOx-TiO₂ [66]. These transients are shown in Fig. 10 at different pulse delay times as a function of wavelength [37].

Due to the femto-second pulses, only FeOx absorbs laser pulses leading to the separation of the cb(e⁻) and vb(h⁺) or excited d-d states. Fig. 10 also shows that the spectral features are about the same for different delays. An increase in the pulse delay up to 500 ps, leads to a decrease in absorption bands. Additional experiments showed that the main part of the absorption amplitude at 600 nm decays within 25 ps ($t_{1/2} \sim 25$ ps). Mid-gap Fe d-d states have been suggested as the main trapping sites with lifetimes of a few hundred picoseconds and these d-d states are ascribed to local excitons in the FeOx matrix [37]. Fig. 10 indicates also that the electron trapping process was initiated at times of 150 fs and will compete with electron-hole recombination. The absorption band with a maximum at 600 nm was assigned to the cb(e⁻) spectrum of the FeOx-TiO₂ [66,72–74]. Until now, no unambiguous identification for the FeOx or TiO₂ in the FeOx-TiO₂ spectrum has been reported [37,65,69]. In the case of TiO₂ photosensitization, electron lifetimes <100 fs have been reported by electron injection experiments [75].

A loss of photo-induced electron absorption due to electron trapping and charge recombination significantly decreases the electron injection signals. A second factor decreasing the electron injection signals due to the depletion of the FeOx ground-state electrons. This happens because of the electrons jumping from the ground state to higher excited energetic states. These results suggest that the bleaching observed <405 nm in Fig. 10, shifts the absorption bands to shorter wavelength, probably involving the Kerr effect [35–37,66]. At any rate, the bleaching <400 nm involved FeOx modified by TiO₂ low-lying surface states [37,76,77].

5. Conclusions

The present review addresses the bacterial disinfection activated by UV-sensitive films like PE-TiO₂ progressively moving to

visible light activated transparent films. Contact angle determination allowed the quantitative determination of the photo-switching rates related to bacterial inactivation. The synthesis, material chemistry and microstructure of innovative PE-FeOx films were reported in this review. The efficient bacterial inactivation proceeding with acceptable kinetics shows a potential for the future application of these films inducing repetitive bacterial disinfection. This aspect is especially important on PE where bacteria develop easily with the known adverse effects. A mechanism for the photocatalytic disinfection by PE-FeOx was suggested consistent with the experimental work.

Femto-second spectroscopy was employed to report the generation of transients in PE-FeOx-TiO₂ under 545 nm/25 fs femto-second pulses. Transient decay comprised ultrafast charge recombination, charge separation, charge trapping and low-lying trapping states in TiO₂. This study showed that ~10% of the transients generated > 500 ps by the femto-pulse laser were available to induce at later stages bacterial inactivation in the minute range. Since FeOx and TiO₂ have been co-sputtered on PE, no scheme accounting for the direction of the electron or charge injection is possible since a random distribution of FeOx and TiO₂ were sputtered on the PE film. The *E. coli* inactivation kinetics was the same under the full sunlight emission or after insertion of a 400 nm cut-off filter allowing only visible radiation to reach the surface of the PE-FeOx-TiO₂ film. This observation lends further support to the photosensitizing role FeOx in PE-FeOx-TiO₂ films providing the proof that FeOx random deposition by sputtered films leads to photoactive films in the visible region. These antibacterial films can reduce/eliminate biofilm formation in public places like hospitals/healthcare facilities and their adverse effects involving the spreading of pathogens leading to hospital-acquired infections (HAIs).

The deposition of adhesive antibacterial films showing stable, fast and repetitive microbial degradation is gaining importance due to the increasing resistance of infections by MRSA and *P. aeruginosa* bacteria, both having no effective antibiotic product in the market. More advanced and faster antibacterial composite films active in the dark and under light could inactivate instantly toxic bacteria in hospitals, schools and public places. Biofilms are the most dangerous way to spread infections into the environment of health facilities and their decease should help to bring down the increasing rate of hospital acquired infection (HAI) now affecting 5–10% of the population frequenting hospitals for ambulatory treatment or periods of hospitalization.

Acknowledgements

We thank the EPFL, the Swiss National Science Foundation (SNF) Project (200021-143283/1) and the EC7th Limpid FP project (Grant No 3101177).

References

- [1] A. Fujishima, T. Rao, D. Tryk, *J. Photochem. Photobiol. C* 1 (2000) 1–21.
- [2] J. Schneider, M. Matsuoka, M. Takeuchi, J. Zhang, Y. Horiuchi, M. Anpo, D. Bahnemann, *Chem. Rev.* 118 (2014) 9919–9983.
- [3] W. Daoud, *Self-cleaning Materials and Surfaces*, Wiley & Sons Ltd, UK, 2013.
- [4] A. Bozzi, T. Yuranova, J. Kiwi, *J. Photochem. Photobiol. A* 172 (2005) 27–34.
- [5] A. Mills, J. Hepburn, D. Hazafy, C. O'Rourke, J. Krysa, M. Baudys, M. Zlamal, H. Bartkova, C. Hill, K. Winn, M. Simonsen, E. Soggaard, S. Pillai, N. Leyland, R. Fagan, F. Neumann, C. Lampe, T. Graumann, *J. Photochem. Photobiol. A* 271 (2013) 18–20.
- [6] L. Zhang, R. Dillert, D. Bahnemann, M. Vormoor, *Energy Environ. Sci.* 5 (2012) 7491–7507.
- [7] O. Baghrice, S. Rtimi, C. Pulgarin, C. Roussel, J. Kiwi, *Appl. Catal. B* 130/131 (2013) 65–72.
- [8] O. Baghrice, S. Rtimi, R. Sanjines, C. Pulgarin, J. Kiwi, *J. Photochem. Photobiol. A* 261 (2013) 52–63.
- [9] T. Yuranova, A. Rincon, D. Laub, J. Kiwi, *Catal. Today* 121 (2007) 109–117.

[10] C. Chan, T. Ko, H. Hiroaka, *Surf. Sci. Rep.* 24 (1996) 1–54.

[11] J. Kassanen, M. Suvanto, T. Pakkanen, *J. Appl. Polym. Sci.* 119 (2007) 2235–2245.

[12] A. Bozzi, T. Yuranova, I. Guasaquillo, D. Laub, J. Kiwi, *J. Photochem. Photobiol. A* 174 (2005) 156–164.

[13] S. Rtimi, C. Pulgarin, R. Sanjines, J. Kiwi, *RSC-Adv.* 3 (2013) 16345–16348.

[14] P.J. Kelly, R.D. Arnell, *Vacuum* 56 (2000) 159–172.

[15] K. Page, M. Wilson, I.P. Parkin, *J. Mater. Chem.* 19 (2009) 3819–3831.

[16] A. Mills, C. Hill, P. Robertson, *J. Photochem. Photobiol. A* 237 (2012) 7–23.

[17] H.A. Foster, P. Sheel, D.W. Sheel, P. Evans, S. Varghese, N. Rutschke, J.H.M. Yates, *J. Photochem. Photobiol. A* 216 (2010) 283–289.

[18] P.S.M. Dunlop, P.C. Sheeran, M.J.A. Byrne, S.A.M. McMahon, M.A. Boyle, G.K. McGuigan, *J. Photochem. Photobiol. A* 216 (2010) 303–310.

[19] H.M. Yates, L.A. Brook, I.B. Ditta, P. Evans, A.H. Foster, D.W. Sheel, A.J. Steel, *J. Photochem. Photobiol. A* 197 (2008) 197–205.

[20] S. Rtimi, R. Sanjines, M. Andrzejczuk, C. Pulgarin, A. Kulik, J. Kiwi, *Surf. Coat. Technol.* 254 (2014) 33–343.

[21] M. Pelaez, N. Nolan, S. Pillai, M. Seery, P. Falaras, A. Kontos, M.S.P. Dunlop, J. Hamilton, J.-A. Byrne, K. O'Shea, M. Enterazi, D. Dionysiou, *Appl. Catal. B* 25 (2012) 331–349.

[22] D. Keane, K. Mc Guigan, P. Fernandez, I. Polo-Lopez, J.-A. Byrne, P.S.M. Dunlop, K. O'Shea, D. Dionysiou, S.C. Pillai, *Catal. Sci. Technol.* 4 (2014) 12111–12121.

[23] J.A. Byrne, P.S.M. Dunlop, J. Hamilton, P. Fernandez-Ibanez, I. Polo Lopez, P. Sharma, A. Vennard, *Molecules* 20 (2015) 5574–5615.

[24] G. Walters, P.I. Parkin, *J. Mater. Chem.* 19 (2009) 574–590.

[25] S. Rtimi, C. Pulgarin, R. Sanjines, J. Kiwi, *RSC Adv.* 5 (2015) 80203–80211.

[26] R. Bauer, G. Waldner, S. Hager, T. Krutzler, S. Malato, P. Maletzky, *Catal. Today* 53 (1999) 131–144.

[27] J. Ndounla, S. Spuhler, S. Kenfak, J. Wethe, C. Pulgarin, *Appl. Catal. B* 129 (2013) 309–317.

[28] R. Ruales-Lonfat, N. Bentez, A. Sienkiewicz, C. Pulgarin, *Appl. Catal. B* 160 (2014) 286–297.

[29] S. Dancer, *J. Hosp. Infect.* 73 (2009) 378–386.

[30] I. Kramer, I. Schwebke, G. Kampf, *BMC Infect. Dis.* 6 (2006) 137–146.

[31] R. Noimark, S. Dunhill, Ch. Wilson, I.P. Parkin, *Chem. Soc. Rev.* 38 (2009) 3435–3448.

[32] A.Y. Peleg, D.C. Hooper, *Hospital-Acquired infections due to gram-Negative bacteria*, *N. Engl. J. Med.* 362 (2010) 1804–1813.

[33] D. Adams, L. Brus, C. Chidsey, S. Creager, C. Creutz, P. Ch Kagan, M. Kamat, S. Lieberman, R. Lindsay, R. Marcus, Metzger M. Michel-Beyerle, J. Mille, M. Newton, D. Rolison, O. Sankey, K. Schanze, Z. Yardley, X. Zhu, *J. Phys. Chem. B* 107 (2003) 6668–6680.

[34] W. Zhou, H. Fu, K. Pan, C. Tian, Y. Qu, *J. Phys. Chem. C* 112 (2008) 19584–19590.

[35] Y. Cong, Z. Li, Y. Zhang, Q. Wang, Q. Xu, *Chem. Eng. J.* 191 (2012) 356–363.

[36] B. Palanisamy, C. Babu, B. Sundarevel, S. Anandan, V. Murugesan, *J. Hazard. Mater.* 252 (2013) 233–240.

[37] S. Rtimi, R. Sanjines, J. Kiwi, C. Pulgarin, M. Bensimon, I. Khmel, V. Nadtochenko, *RSC Adv.* 5 (2015) 101751–101759.

[38] M. Horng, J. Gardecki, A. Papazyan, M. Moroncelli, *J. Phys. Chem.* 99 (1995) 17331–17340.

[39] W. Pollard, B. Brito-Cruz, C. Shank, R. Mathies, *J. Chem. Phys.* 90 (1989) 199–206.

[40] L. Fu, Z. Wu, X. Ai, J. Zhang, Y. Nie, S. Xie, G. Yang, B. Zou, *J. Chem. Phys.* 120 (2004) 3406–3411.

[41] M.I. Mejia, J.M. Marin, G. Restrepo, C. Pulgarin, J. Kiwi, *Catal. Today* 161 (2011) 15–22.

[42] J. Nesic, S. Rtimi, D. Laub, G.M. Roglic, C. Pulgarin, J. Kiwi, *Colloids Surf. B: Biointerfaces* 123 (2014) 593–599.

[43] S. Rtimi, J. Nesic, C. Pulgarin, R. Sanjines, M. Bensimon, J. Kiwi, *Interface Focus* 5 (2015) 20140046.

[44] J. Mathews, *Epitaxial Growth, Part B*, IBM Thomas Watson Res. Center, Academic Press, New York, 1975, pp. 382–436.

[45] R. Wang, K. Hashimoto, A. Fujishima, A. Chikuni, M. Kojima, E. Kitamura, A. Shimohigishi, M. Watanabe, *Nature* 388 (1997) 431–432.

[46] N. Saka, R. Wang, A. Fujishima, T. Watanabe, K. Hashimoto, *Langmuir* 14 (1998) 5918–5920.

[47] K. Seki, N. Tachiya, *J. Phys. Chem.* 108 (2004) 4806–4810.

[48] O. Baghrache, S. Rtimi, A. Zertal, C. Pulgarin, R. Sanjines, J. Kiwi, *Appl. Catal. B: Environ.* 174 (2015) 376–382.

[49] P. Maness, S. Smolinski, D. Blake, Z. Huang, E. Wolfrum, W. Jacoby, *Appl. Environ. Microb.* 65 (1999) 4094–4098.

[50] S. Parra, I. Guasaquillo, O. Enea, E. Mielczarski, J. Mielczarski, P. Albers, L. Kiwi-Minsker, J. Kiwi, *J. Phys. Chem. B* 107 (2003) 7026–7035.

[51] M. Dhananjeyan, J. Kiwi, R. Thampi, *Chem. Comm.* (2000) 1443–1444.

[52] P. Docampo, S. Guldin, U. Steiner, H.J. Snaith, *J. Phys. Chem. Lett.* 4 (2013) 698–703.

[53] Y.L. Jayachandranand, S.K. Narayandass, *Trends Biomater. Artif. Organs* 24 (2010) 90–93.

[54] C.D. Wagner, M.W. Riggs, E.L. Davis, G.E. Müllenber (Eds.), *Handbook of X-Ray Photoelectron Spectroscopy*, Perkin-Elmer Corporation Physical Electronics Division, Minnesota, 1979.

[55] A.D. Shirley, *Phys. Rev. B* 5 (1972) 4709–4716.

[56] J. Nogier, M. Delamar, P. Ruiz, M. Gratzel, R. Thampi, J. Kiwi, *Catal. Today* 20 (1994) 109–123.

[57] J. Kennedy, A. Bard, *J. Electrochem. Soc.* 125 (1978) 723–726.

[58] D.M. Stabury, *Adv. Inorg. Chem.* 33 (1989) 69–138.

[59] K. Hardee, A. Bard, *J. Electrochem. Soc.* 125 (1978) 215–233.

[60] M.I. Litter, J.A. Navio, *J. Photochem. Photobiol. A* 98 (1996) 171.

[61] K. Nagaveni, M.S. Hedge, G. Madras, *J. Phys. Chem. B* 108 (2004) 20204.

[62] Wei Zhou, Wei Li, Jian-Qiang Wang, Yang Qu, Ying Yang, Ying Xie, Kaifu Zhang, Lei Wang, Honggang Fu, Dongyuan Zhao, *Adv. Funct. Mater.* 21 (2011) 1922–1930.

[63] Wei Zhou, Fanfei Sun, Kai Pan, Guohui Tian, Baojiang Jiang, Zhiyu Ren, Chungui Tian, Honggang Fu, *J. Am. Chem. Soc.* 136 (2014) 9280–9283.

[64] S. Rtimi, R. Sanjines, C. Pulgarin, A. Houas, J.-C. Lavanchy, J. Kiwi, *J. Hazard. Mater.* 260 (2013) 860–868.

[65] Sami Rtimi, Martin Robyr, César Pulgarin, Jean Claude Lavanchy, John Kiwi, *J. Catal.* 342 (2016) 184–192.

[66] Sami Rtimi, Cesar Pulgarin, Victor A. Nadtochenko, Fedor E. Gostev, Ivan V. Shelaev, John Kiwi, *Sci. Rep.* 6 (2016) (Article number: 30113).

[67] S. Leytner, J.T. Hupp, *Chem. Phys. Lett.* 330 (2000) 231–239.

[68] D.C. Hurum, A.G. Agrios, S.E. Crist, K.A. Gray, T. Rajh, M.C. Thurnauer, *J. Electron. Spectrosc. Related Phenom.* 150 (2006) 150–158.

[69] S. Pendlebury, X. Wang, F. Le Formal, M. Cornuz, A. Kafizas, S. Tilley, M. Gratzel, J. Durrant, *J. Am. Chem. Soc.* 136 (2014) 9854–9857.

[70] B.C. Fitzmorris, J.M. Patete, J. Smith, X. Mascorro, S. Adams, S.S. Wong, J.Z. Chang, *ChemSusChem* 6 (2013) 1907–1913.

[71] V. Nadtochenko, N. Denisov, O. Sarkisov, D. Gumi, C. Pulgarin, J. Kiwi, *J. Photochem. Photobiol. A* 181 (2006) 401–410.

[72] J. Cherepy, P. Moore, A. Mathies, *J. Phys. Chem. B* 101 (1997) 3250–3256.

[73] A. Joly, J. Williams, A. Chambers, G. Xiong, W. Hess, D. Laman, *J. Appl. Phys.* 99 (2006) 053521.

[74] N. Geoffrey, *Introduction to Nonlinear Optics*, Cambridge University Press, 2016 (ISBN 978-1-139-500760).

[75] D. Wheeler, G. Wang, Y. Ling, Y. Li, J. Zhang, *Energy Environ. Sci.* 5 (2012) 6682–6889.

[76] Sami Rtimi, Cesar Pulgarin, Martin Robyr, Arseniy Aybush, Ivan Shelaev, Fedor Gostev, Victor Nadtochenko, John Kiwi, *Appl. Catal. B Environ.* 208 (2017) 135–147.

[77] Sami Rtimi, *Catalysts* 7 (2017) 57.